High-temperature deformation and consolidation of polycrystalline α-SiC by spark plasma sintering

Dmytro Demirskyi (a, b, c), Hossein Sepehri-Amin (a), Oleg O. Vasylkiv (a)*

(a) National Institute for Materials Science, 1-2-1 Sengen, Tsukuba, Ibaraki 305-0047, Japan

(b) WPI-Advanced Institute for Materials Research (WPI-AIMR), Tohoku University, 2-1-1 Katahira, Aoba-ku, Sendai, 980-8577 Japan

(c) Faculty and Graduate School of Maritime Sciences, Kobe University, 5-1-1 Fukaeminami-machi, Higashinada-ku, Kobe 658-0022, Japan

* Author to whom correspondence should be addressed, Oleg Vasylkiv oleg.vasylkiv@nims.go.jp

**Dmytro Demirskyi and Oleg Vasylkiv contributed equally to this study.

Abstract

The main objective of this investigation is the consolidation and flexural strength of alpha silicon carbide ceramics produced without additives by spark plasma sintering. Using the design of the experiment method, we optimized temperature and dwell to achieve fully dense silicon carbide bulks. The consolidation process of silicon carbide was analyzed similarly to the creep of bulk ceramics, and it was determined that the activation energy for the densification process was 596±39 kJ/mol, while the stress exponent *n* was below 2. Bulk additive-free silicon carbide ceramics gradually increased flexural strength as the temperature rose to 2000 °C. The flexural strength at 2000 °C was influenced by the loading rate, and under 2.5 mm/min, it reached a maximum of 2.08 GPa. To explain this phenomenon, a deformation mechanisms map was created, indicating that diffusion creep is the most probable mechanism for the strain sensitivity of SiC at 2000 °C. Transmission electron microscopy indicated a substantial rise in twin density within the α-SiC grains at 2000 °C, indicating the activation of a previously unreported self-reinforcing mechanism.

Keywords: Polycrystalline α-SiC; High temperature deformation; spark plasma sintering; microstructure

1 Introduction

Bulk silicon carbide ceramic or SiC-based ceramics are one of the most used ceramics in a wide range of structural applications owing to their relatively low specific density (3.21 g/cm^3), high hardness (>24 GPa), and high Young's modulus (420 GPa) [1–4]. The majority of the commonly applied characteristics of silicon carbide are derived from its unique structure and bonding properties. This ceramic showcases predominant covalent bonds among C–Si, Si–Si, and C–C atoms in the crystal cell, which can exhibit cubic, hexagonal, or rhombohedral configurations [5,6]. Hexagonal and rhombohedral silicon carbide can manifest diverse polytypes where atoms align uniformly in two dimensions but vary in the third dimension. These layers can be structured in three distinct configurations: A, B, or C, to attain the highest degree of packing efficiency.

The covalent nature of the bonds in silicon carbide makes it quite difficult to manufacture using the powder metallurgy approach, i.e., by pressing and sintering, as sintering temperatures exceeding 2000°C would be required [7–9]. At these temperatures, silicon carbide undergoes three competing processes: densification, grain growth, and polymorphic transformation [10]. The use of an inappropriate sintering medium or slow heating to sintering temperature would lead to the development of a coarse grain structure, potentially impeding densification beyond 90% of theoretical density (TD).

To overcome these challenges, one can utilize the following methods: (i) reducing the particle size of the initial SiC powder (i.e., ultrafine or nanopowders) [11]; (ii) adding sintering additives such as B, Al, C [12]; (iii) employing liquid phase sintering [13] or (iv) utilizing pressure-assisted approaches like hot-pressing (HP) or

spark plasma sintering (SPS) [14–16]. Because there should be a phase β→α phase transformation, if the cubic silicon carbide (β-SiC) powder is being used for consolidation, the processing at temperatures above 2000 °C may cause the appearance of elongated grains, affecting the mechanical performance of silicon carbide. Another issue can be the presence of the surface SiO_2 layer [5]. In order to reduce this thin layer during the densification process, the addition of carbon is commonly used. Noticeably, Prochazka and Scanlan [17] succeeded in the densification of β-SiC by pressureless sintering using boron and carbon as an additive and fine SiC powder (specific surface area 9 m^2/g). Sintering at 2020 °C resulted in a relative density of 94–96% of TD. Alliegro et al. hot-pressed silicon carbide to 98% of TD using various additives, including 1 wt.% of Al. [14].

Using hot pressing at 1950°C and boron carbide as a sintering additive, Bind and Biggers were able to produce almost fully dense silicon carbide [15]. They observed that the resulting composition was a cubic silicon carbide matrix with 6H or 2H polytype inclusions. The presence of a liquid phase during liquid phase sintering encourages the transformation from beta to alpha phase, leading to improved fracture toughness and the development of α-SiC platelets in the microstructure. Nevertheless, the presence of a liquid phase during the sintering of silicon carbide can result in the formation of disordered silicate compounds at the boundaries between grains and their accumulation at the junctions of three grains. These factors will determine the maximum temperature at which the material can be used effectively, and typically, silicon carbide ceramics sintered with a liquid phase exhibit poorer creep resistance compared to those produced through solid-state sintering methods [5].

Alternatively, one can use as few additives as possible or the multistep consolidation procedure in the case of the β-SiC [18]. Kim et al. [19] thus reported that flexural strength remains quite high up to 2000°C, where the plastic strain-stress curves were observed. Sajgalic et al. [20] suggested that additive-free processing results in Vickers hardness of 29 GPa and creep resistance at 1450°C comparable to that of

commercial α-SiC sintered at 2150°C.

To the authors' knowledge, only Maitre et al. [21] reported additive-free processing of α-SiC ceramic by SPS. Densification at 1950°C using a 5-min dwell resulted in 97.5% of TD density. This was mainly possible due to the extremely fine starting powder (specific surface area 26.7 m^2/g). However, this study did not report any details on the mechanical properties, but it indicated that rapid densification can be associated with diffusion mechanisms through melt or a time-independent process such as plastic deformation.

Therefore, the main objectives of this study are: (a) to create dense silicon carbide utilizing α-SiC powder, (b) to examine the factors that influence the densification process, and (c) to evaluate their flexural strength at temperatures reaching 2000°C. We used a commercial α-SiC powder in combination with SPS employing a linear ramp-and-hold profile, with densification temperatures ranging from 1900°C to 2100°C. After the trial runs, the processing parameters were assessed using an experimental design methodology, focusing on optimizing density, average grain size, and the presence of the 15R polytype. Finally, we performed a flexural strength test using a three-point and a four-point configuration and characterized the microstructure of the specimens showing the highest strength by transmission electron microscopy (TEM).

2 Materials and Methods

2.1 Details on the initial powder

The starting powder was fine α-SiC powder with a mean particle size of 0.61 μm (OY–15, Yakushima Denko Co., Ltd., Tokyo, Japan). This powder was from a 3 kg batch with the following impurities: Fe < 300 ppm, Al < 200 ppm and SiO_2 up to 7800 ppm in wt.%. These were measured by the supplier using the JIS R 6124 standard procedure. The untreated α-SiC powder was used for the densification studies. Several studies attempted to consolidate α-SiC without additives, and, in

general, copying thermal profiles from previous studies could result in inadequate density and, thus, mechanical performance. Therefore, within this study, we made a systematical evaluation of the temperature and dwell time during the spark plasma sintering process through statistical planning of experiments, i.e., ‘experimental design' or design of experiments (DoE) approach [22–24]. The DoE is a statistical method used to determine the relation between the processing parameters and the response of the preset experimental output variable, assuming that there is a direct influence/correlation between them. Using the experimental design approach, it is possible to establish a combination of the experimental variables that produce the best response values.

In this study, we utilized a polynomial response surface incorporating the 'function of desire response' [24] to determine the optimal values and their relationship with processing parameters, which was successfully achieved through 22 experiments (refer to *Suppl. S*1).

2.3 Spark plasma sintering procedure

The untreated powders were placed in the SPS graphite die. We used an inner Ta-foil (Sigma-Aldrich Chemie, 0.025 mm thick, 99.9+% metal basis) and outer graphite foil configuration in which the Ta-foil is used to isolate the powder mixture from the graphite felt or the graphite die. Thus, the hollow tantalum cylinder was filled with the powder mixture. The top and bottom of such a cylinder were covered with two circular cut-outs made from the tantalum foil. These steps are necessary to minimize the diffusion of carbon [25] into the powder mixture during the SPS process. Tantalum foil will form the ~50 μm tantalum carbide layer during the SPS process [26]. The SPS experiments were conducted using the ‘Dr. Sinter’ 1050 (Sumitomo, Japan) unit with a 25-mm or 30-mm die.

The schedule for the specimens used for the high-temperature flexural tests includes the following major steps: (step 1) heating the samples to 800 °C in 4 minutes,

following (step 2) 26 min heating to the densification temperature of between 1900 °C and 2100 °C. At the sintering temperature, a 15 to 50-minute dwell (step 3) was used as a homogenizing step. (step 4) cooling to 1800 °C in 5 minutes, then to 600 °C in 40 minutes. The pressure of 45 MPa was maintained during the heating, consolidation, and cooling stages. Argon gas at the flow rate of 2 L/min was used. The temperature and duration of step 3 were optimized using DoE methods.

2.4 Characterization of silicon carbide

After coarse grinding, the sintered specimens were polished with diamond disks with a particle size of up to 0.5 μm. The density of the samples was measured by the Archimedes method using water or ethanol as the medium in accordance with ASTM B 962–08.

An X-ray diffraction (XRD) analysis (D8 Advance, Bruker, Karlsruhe, Germany) was performed on the polished surfaces of the bars after the flexural tests using Cu-Kα radiation. The intensity data were collected over the 2θ range of 30°–80° in steps of 0.02° using a sampling time of 10 s for each step. The software used for refinement was TOPAS (TOPAS Ver. 4.2, Bruker AXS, Germany) or Profex [27]. Instrumental broadening was determined using a NIST 660b LaB_6 standard run under the same conditions for each sample.

The three-point flexural strength was determined using rectangular blocks (1.5×2×25 mm, ASTM C1211−13, configuration B) and the strength testing equipment that was previously described in detail [28]. A span of 16 mm was used. Unless stated otherwise, the flexural strength data were averaged based on eight tests. In some cases, additional tests using the four-point flexure method were performed. For the four-point tests, the 20/10 configuration was used.

The hardness was determined by a Vickers hardness tester (Akashi, AVK-A, Japan) using loads of 49, 98, and 196 N with a dwell time of 15 s following the standard procedure (ASTM C 1327–15). The indentation fracture toughness was calculated using the half length of the crack formed around the corners of indentations at the

load of 196 N using the following equations developed by Anstis et al. [29] or Lawn and Fuller [30].

The microstructure of the silicon carbide ceramics was studied by scanning electron microscopy (SEM, JCM-6000, JEOL). Scanning transmission electron microscopy (STEM) was performed using a Titan G2 80–200 (FEI) equipped with a probe aberration corrector and an energy-dispersive X-ray spectrometer (EDS).

3 Results and Discussion

3.1 Optimization of the SPS processing

In order to find the best processing conditions for the fully dense silicon carbide, we performed a set of experiments using a factorial design approach with an additional center point [23]. **Figure 1** shows the contours for the linear regression performed using specimens of different sizes. It is clear that the nature of the response of the density to temperature and dwell time differs significantly when experimenting with specimens with a slight distinction in diameter. This is due to temperature distribution inside a die during the SPS process [31].

Based on the results in **Figure 1,** it was decided to fabricate specimens for high-temperature tests using a 2010°C/20 min configuration, which was not used during the screening process. The bulk and relative density of these specimens were 3.208 g/cm^3 and 99.80% of TD, respectively.

This shows a decent proximity with that expected by a model. As can be seen from **Fig. 1 (b)**, the path for the fully dense bulk silicon carbide lies with 20–25 min dwell using 2010–2050 °C. Going beyond this area will gradually lead to a decrease in density. Alternatively, one can use a 2050°C/48 min configuration for preparing SiC using a 30-mm die (**Fig. 1(b)**). Such an effort will result in a coarser grain size, but a density higher than 3.2 g/cm^3 can be obtained.

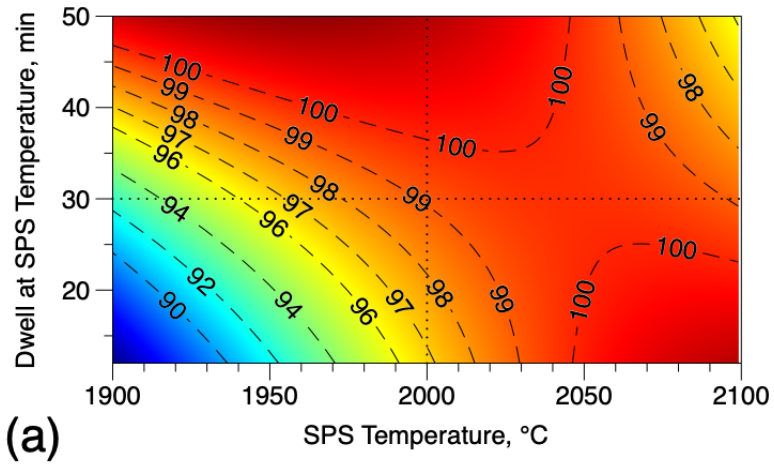

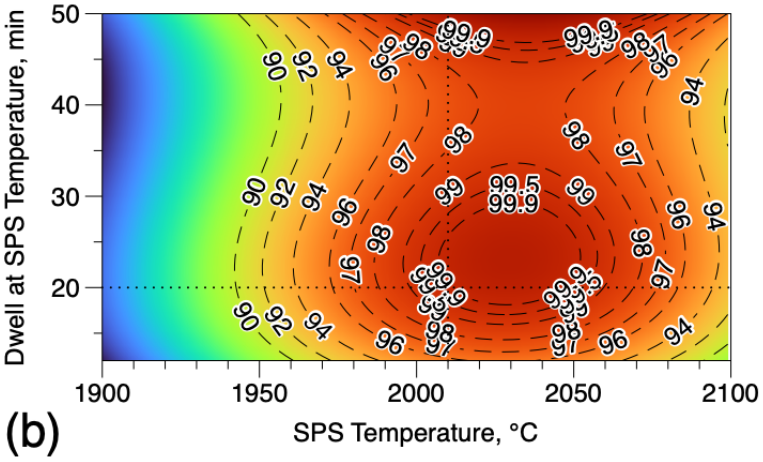

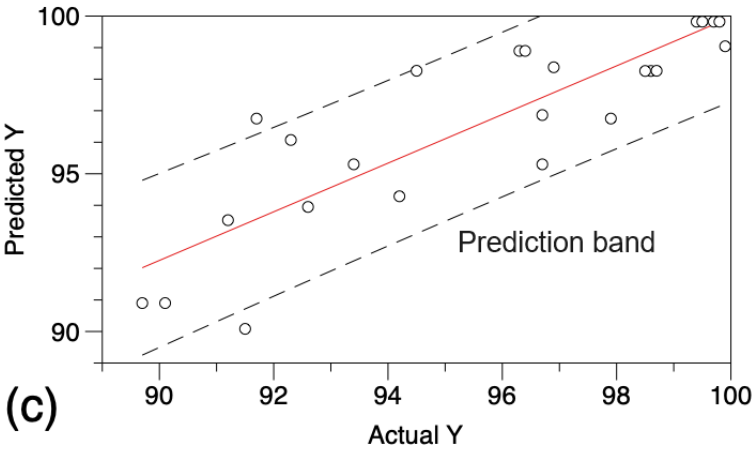

Figure 1: Response surface representation of the relative density of the SPSed silicon carbide ceramics. The dotted lines show the initial 2000/30 or 2010/20 configurations. (a) is for the specimens using a 25-mm die, and (b) is for the 30-mm die. (c) shows the relation between the observed density values and those forecasted by the linear regression model presented in (b).

3.2 Densification kinetics of SiC

The shrinkage data during the sintering process can be used to identify the dominant consolidation mechanism. For silicon carbide, we found only two studies that were focused on the densification behavior of SiC [10,15]. Bind and Biggers [15] analyzed the densification process of SiC containing 1 wt.% B_4C during the HP process. They used the approach of Murray et al. [32], which allows the activation energy for sintering to be calculated using apparent viscosity at selected processing conditions. Bind and Biggers [15] reported that the activation energy for hot-pressing was 481±75 kJ/mol. They concluded that viscous flow was the main mechanism controlling densification between 1750°C to 1950°C.

Lodhe et al. analyzed the spark plasma sintering of silicon carbide using a polycarbon silicate as SiC precursor [10]. Their work focused on densification and β→α phase transformation. They used the model proposed by Bernard-Granger and Guizard [33] for their analysis. This model is based on the creep deformation process of bulk ceramics, which should satisfy the following:

$$\dot{\varepsilon} = \frac{d\varepsilon}{dt} = A\frac{DG_0\boldsymbol{b}}{kT}\left(\frac{\boldsymbol{b}}{d}\right)^p\left(\frac{\sigma_{macro}}{G_0}\right)^n \text{(eq. 1)}$$

where ε_{rate} is creep rate, A – constant, D – diffusion coefficient, G_0 – shear modulus, $\boldsymbol{b}$ – the Burgers vector, k – Boltzmann's constant, T – absolute temperature, d – grain size, σ_{macro} macroscopic applied stress, *p* – inverse grain size exponent, and *n* is stress exponent, while *t* is time.

Using a densification rate of 1×10^{-4} s^{-1} Lodhe et al. [15] analyzed the densification of silicon carbide ceramics containing both the α-SiC and β-SiC. They evaluated that *n* in eq (1) should be higher than 2 (i.e., dislocation-based mechanism), and they reported the activation energies for the SPS process between 232 and 415 kJ/mol.

Within this study, we also applied this approach, while the key parameters for the (eq.1) were green density 60% of TD, G0 = 182 GPa, Poisson's ratio 0.21, and σ_{macro}= 45 MPa.

It is widely recognized that silicon carbide, being a covalent ceramic, will experience

limited shrinkage during the densification stage. The addition of different additives during the processing of α-SiC can significantly impact its shrinkage characteristics. **Figure 2** illustrates the typical shrinkage curves observed during the SPS, and **Fig. 2 (b)** shows a shrinkage as a function of time at 2010 °C. Here, the shrinkage curves were numerically recalculated in order to satisfy the (eq. 1).

And it was empirically evaluated that the stress exponent n=1.85. The value of the stress exponent at a fixed densification rate varied from 1.56 to 1.91. Using the selected trial points from the SPS screening process and using an identical densification rate as in Lodhe et al. [15] (1×10^{-4} s^{-1}), the data were summarized in **Fig. 3** to evaluate the activation energy for the densification process. Here, the value of the stress exponent obtained for each sintering run was used.

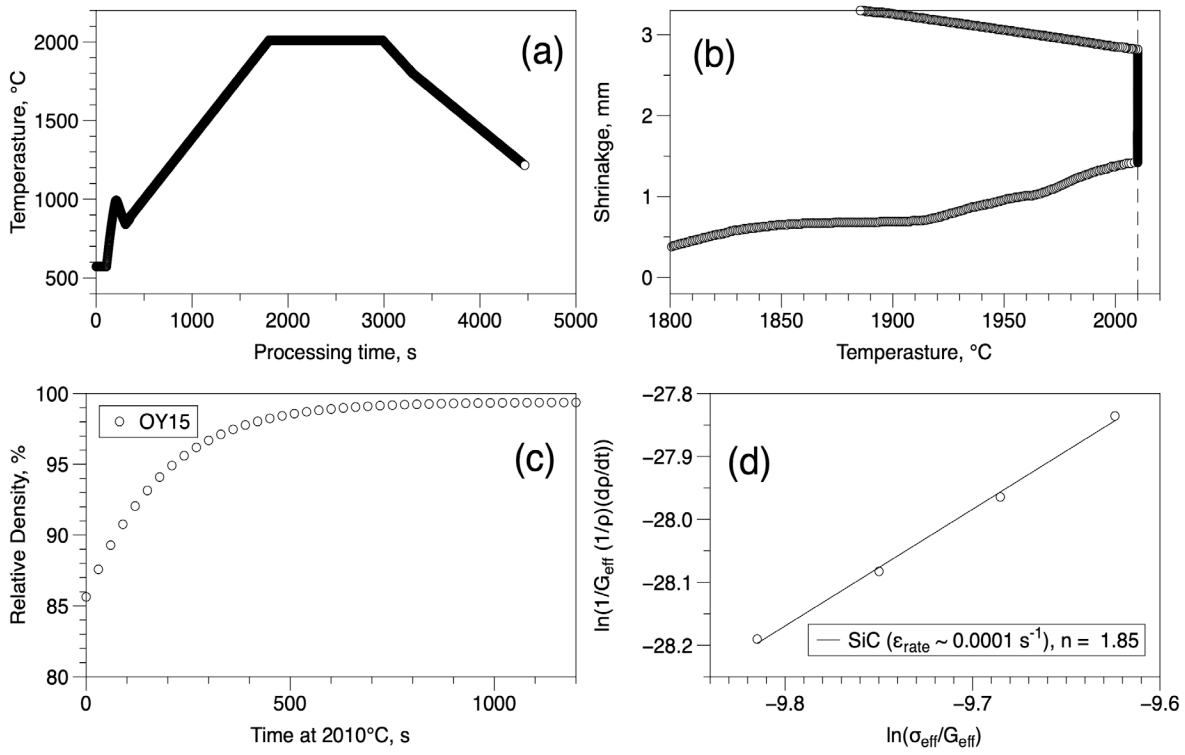

Figure 2: Densification details on α-SiC ceramics during the spark plasma sintering process using a 2010/20 configuration. (a) heating profile, and (b) shrinkage as a function of temperature. (c) shows shrinkage as a function of dwell time at 2010°C, while (d) presents the densification of silicon carbide by the method proposed by Bernard-Granger et al. [33].

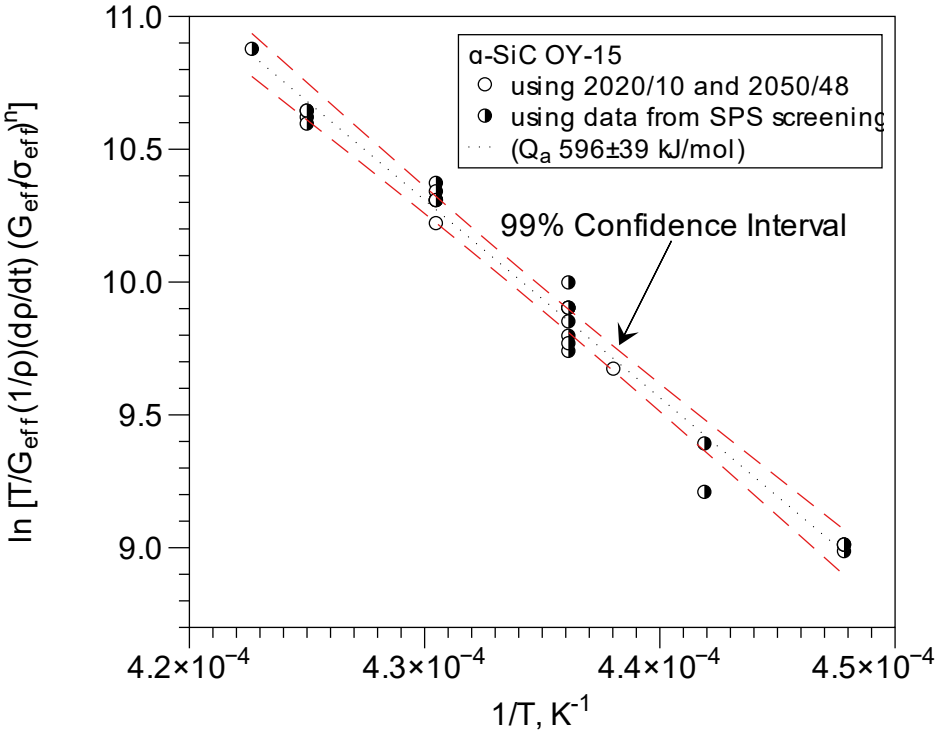

Figure 3: Evaluation of the activation energy for the densification during the SPS process using a fixed pressure of 45 MPa and the densification rate of 1×10^{-4} s^{-1}.

Using a fixed pressure of 45 MPa, we evaluated that the activation energy for the densification process was 596±39 kJ/mol. Which is higher than that reported by Bind and Biggers [10] (481±75 kJ/mol) or Lodhe et al. [15] (415 kJ/mol).

It can be stressed that in the case when *the n value is greater than 2 but less than* 5, it is expected that the densification process should be controlled by the dislocation activity. While $n \sim 2$ should correspond to the diffusion-based densification (or at least the diffusion-based process should contribute substantially as Coble creep or Nabarro-Herring creep have n=1). In the original analysis for the method involving eq (1), Bernard-Granger and Guizard [33] analyzed the rate equation, which has n=2 using a model developed by Burton [35] for the superplastic deformation of a polycrystalline material by grain-boundary sliding. Alternatively, Langdon [36] suggested that for some ceramics, the creep controlled by the grain-boundary sliding should have n=2. At the same time Cannon and Sherby [37] found a considerable contribution of grain-boundary sliding during creep tests on the coarse-grained

alumina (65 μm) while the main mechanism was considered as dislocation creep with n=2.6. Ashby and Verrall [38] also mentioned that the strain rate for diffusion creep for fine grain size is proportional to σ^2/d rather than σ/d^2 or σ/d^3. Here, similar to eq. (1) the σ is the applied stress, and d is the grain size.

At elevated temperatures, the dislocations can overcome the obstacles by glide or climb; however, within this study, after consolidation, only a few intragranular dislocations were observed (see *Sect 3.4.3*). The presence of these dislocations that the grain boundary sliding mechanism has operated during the deformation, we may postulate that the contribution of this mechanism to densification is negligible. In the alternative case, when the dislocation terminates inside the grain, one can presume that the mechanism associated with the stress release during deformation can be expected.

Considering the value of the activation energy is slightly higher than reported by [10] or [15]. Obviously, it is possible that multiple mechanisms are active during the densification process. **Table 1** summarizes the activation energies for the self-diffusion in the SiC and is determined by the analysis of the sintering kinetics [5,10,15]. Because mass transport is expected to be vacancy-based, it is noteworthy that the analysis by van Rijswijk and Shanefield [42] suggested that the excess vapor pressure of the other element enhances the self-diffusion rate of C or Si. One can expect that the presence of carbon monoxide (CO) in the solid-phase sintering process would enhance silicon self-diffusion in silicon carbide [5].

At the same time, several creep studies were performed on the SiC ceramics (including reaction-bonded SiC). These experiments are being presented in the **Table 2** [43–49]. As expected, most of the observations are being made below 1600°C. As a rule, for creep studies, the activation energy for steady-state creep below 1600°C is lower than expected for the boundary diffusion of 14C in SiC (see **Tables 1,2**). However, the value listed in **Table 1** was measured in a highly defective polycrystalline material prepared using chemical vapor deposition. Creep at lower temperatures in this range was likely influenced by grain-boundary diffusion. In

comparison, at higher temperatures, the activation energy for creep was greater than that for self-diffusion through the lattice in pure α-SiC single crystals.

The data for high-temperature tests are limited by the creep in bending by Farnsworth [48] (732.6 kJ/mol) or Francis and Coble [49] (305 kJ/mol). These results are consistent with the data analyzed in this study (596±39 kJ/mol). Comparing these results, one should indicate that within this study, the grain size was smaller than in [48] (1.5 μm vs 26 μm), suggesting that the 100 kJ/mol difference can be associated with a co-occurring GB diffusion. Nevertheless, the assumption could not be verified through the TEM observations.

Table 1: Activation energies for diffusion of ^{14}C, ^{30}Si in SiC [5,10,15]

Diffusing species	Type of the diffusion	Type of the SiC specimen	Qa (kJ/mol)	Reference
^{14}C	Self	single-crystal α-SiC	791±8	[5]
^{14}C	Self	single-crystal α-SiC	715±5	[5]
^{14}C	Self	polycrystalline β-SiC via CVD	842±13	[5]
^{30}Si	Self	single-crystal α-SiC (<0001> direction)	697±6	[5]
^{30}Si	Self	single-crystal α-SiC (<0001> direction)	789±10	[5]
^{30}Si	Self	polycrystalline β-SiC via CVD	911±5	[5]
^{30}Si	Grain-boundary	polycrystalline β-SiC via CVD	536±8	[5]
-	dislocation-based mechanism	polycrystalline α-SiC + β-SiC	232–415	[10]
-	dislocation-based mechanism	polycrystalline α-SiC + β-SiC	481±75	[15]
-	GB sliding	polycrystalline α-SiC	596±39	This study

Table 2: Activation energies determined by creep experiments for silicon carbide ceramics [43–49]

Temperature range, °C	Type of the excrement	Type of the SiC specimen	Qa (kJ/mol)	Reference
1397–1647*	Compressive creep	CVD SiC	175±5	[45]
1397–1647*	Compressive creep	sintered α-SiC	395–434	[43]
1647–1747*	Compressive creep	sintered α-SiC	802–914	[43]
1647–1747*	Compressive creep	reaction bonded SiC	711±21	[43]
1497–1647	Compressive creep	sintered α-SiC	387–541	[44]
1647–1747	Compressive creep	sintered α-SiC	838–877	[44]
1620–1760	Compressive creep	sintered SiC	735–790	[46]
1300–1400	Creep in bending	SiC	146±25	[47]
1900–2200	Creep in bending	Hot-pressed α-SiC	732.6	[48]
1975–2120	Creep in bending	Hot-pressed SiC	305	[49]

* See original publication for details. The authors indicate a shift in the activation energy between 1607°C and 1647°C.

3.3 Grain size and structure analysis of SPSed SiC

The average grain size value had a slightly different distribution when comparing the surface responses for the density and the grain size (**Figs. 1** and **4**). Higher processing time at elevated temperatures should result in a larger grain size value. In this study, any lengthy processing above 2050°C would result in the average grain size value above 2 μm, which is a three-fold increase in the size when compared with the size of the aggregates of the initial power (0.67 μm). Grain size for the 2010/30 and 2050/48 configurations, as observed by the optical microscopy (thermally etched), SEM (fractured and polished), and TEM, were within 1.35±0.4 μm and 2.4±0.5 μm, respectively. Individual histograms for the grain size distribution

observed by SEM are presented in *Suppl. S*2. For the 2050/48 configuration, we observed a statistically significant (up to 8%) of the elongated grains with a roughly 1 to 3 ratio between width and length (i.e., 2 by 6 μm). These were rarely (~1%) present. In the specimen consolidated using 2010/20 configuration.

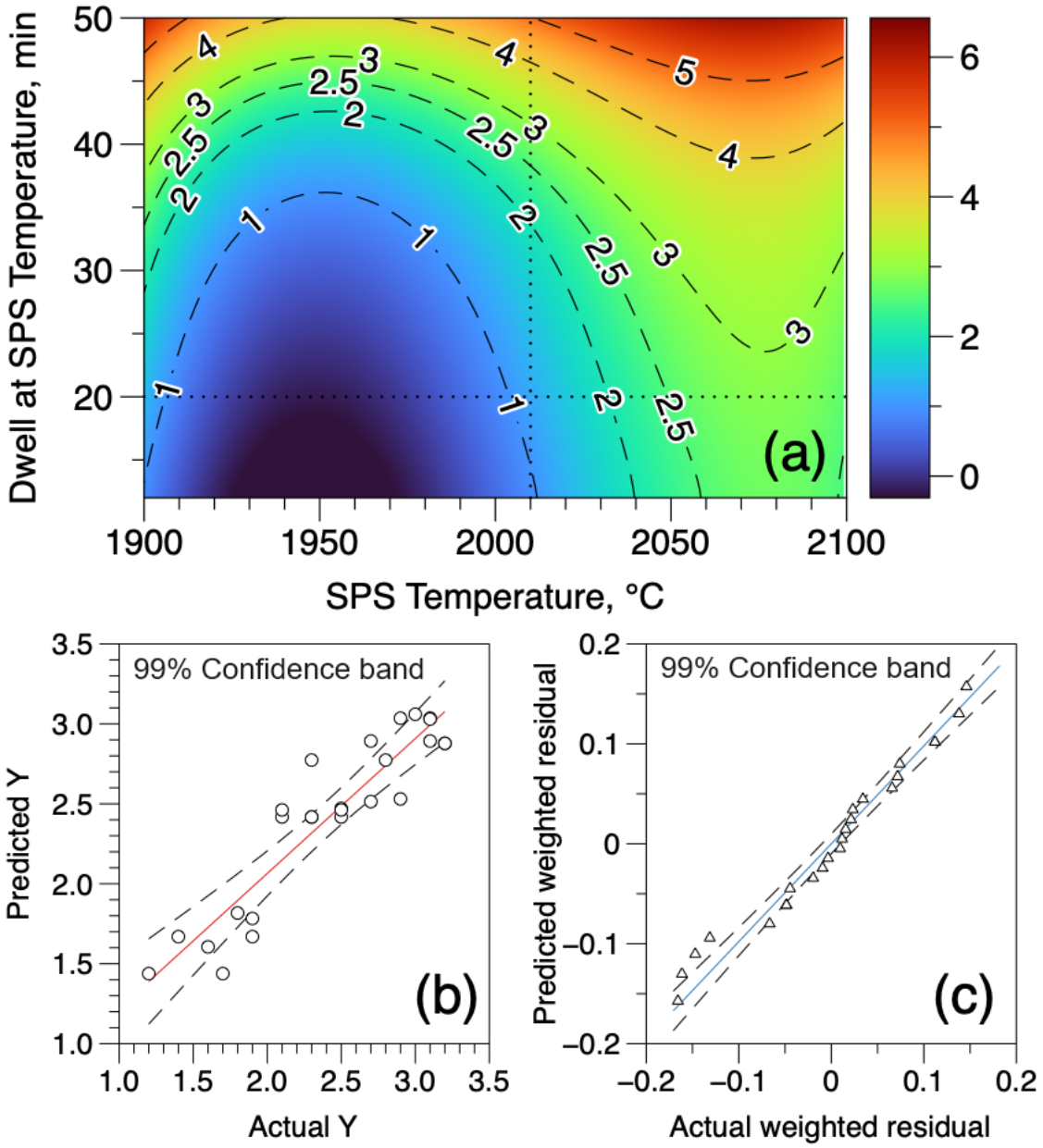

Figure 4: Response surface representation of the grain size of the SPSed silicon carbide ceramics. These silicon carbide specimens were sintered using a 30-mm die and pressure of 45 MPa using OY-–15 powder. The dotted lines show the 2010/20 configuration. (b) compares the actual value of the grain size vs. the predicted value

using a linear regression. The data on the residuals in (c) confirms that the model used for analysis is an adequate one, as data points do not deviate greatly from normal.

3.4 Mechanical properties

As observed in [5,20], additive-free silicon carbide displayed relatively high hardness levels. The hardness was recorded at 31.7±1.1 GPa under a 49 N load. With increasing loads to 96 N and 196 N, the hardness experienced a slight decrease to 28.3±0.2 GPa (for typical SEM see also *Suppl. S*4). These results align with the reported hardness values for various commercial SiC tiles.

Toughness determined by the indentation method was within 2.1–2.5 MPa $m^{1/2}$ and 2.3–2.8 MPa $m^{1/2}$ using approaches by Anstis [29] or Lawn and Fuller [30], respectively. These values are in line with the SiC single-crystals [5] and agree with the data on sintered alpha silicon carbide [50].

Room temperature strength of specimens with density over 98% TD surpassed 600 MPa but seldom exceeded 700 MPa. This finding is in line with Tanaka's analysis of β-SiC [51]. The high-temperature strength was rigorously tested on the 2010/20 specimen, with the 2050/48 specimen as a reference to decrease any error originating from the flexural strength set-up.

From the results on the hardness, toughness, and strength, it is apparent that there is a tradeoff for developing the additive-free alpha silicon carbide ceramic as these bulks have relatively low toughness but higher strength. Considering these bulks' rather good high-temperature performance (*see Section 3.4.1*), one may consider this situation acceptable. Nevertheless, we underline that further improvement in the toughness is suggested as the main goal in further studies on additive-free SiC.

3.4.1 High-temperature flexural strength

The strength of silicon carbide ceramics depends on a number of factors, including

bulk density [16,52], additives used during processing, and starting and final polytype contribution [52]. If silicon carbide ceramics were prepared using the reaction bonding method, infiltration of silicon, or using the liquid phase sintering method, the high-temperature behavior would be limited by the 1400°C/1600°C. Above these temperatures, secondary phases might lead to a sufficient decrease in strength.

Figure 5 shows flexural strength as a function of the temperature of the bulk SiC ceramics developed in this study and compared with those of reported values in the literature [16,19,52–54].

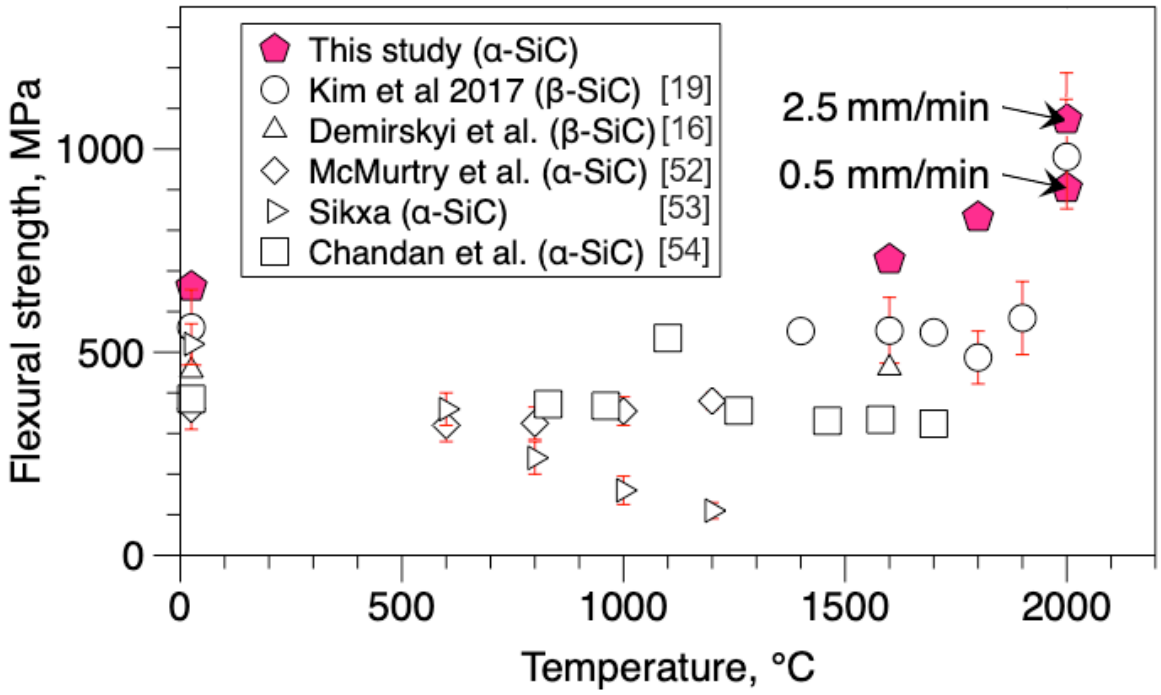

Figure 5: Temperature dependence of silicon carbide ceramics flexural strength [16,19,52–54]. If the error bars are not visible, the error value is smaller than the symbol used for the representation of the average value. The tentative composition is provided, as depending on the processing, the α-SiC may contain the β-SiC [53].

One can already see that there are a few contradicting trends in strength behavior vs temperature: decrease, increase, or almost unchanged strength. The specific mechanisms responsible for these trends are discussed in the refs. [16,19,52–54],

nevertheless, in the case of the unchanged or increase in strength upon an increase in temperature, these can be attributed to the covalent nature of SiC polycrystal and activation of plasticity above 1000 °C [5]. Similar observations for the various shapes of the strength vs temperature curves were reported for boron carbide bulks [54].

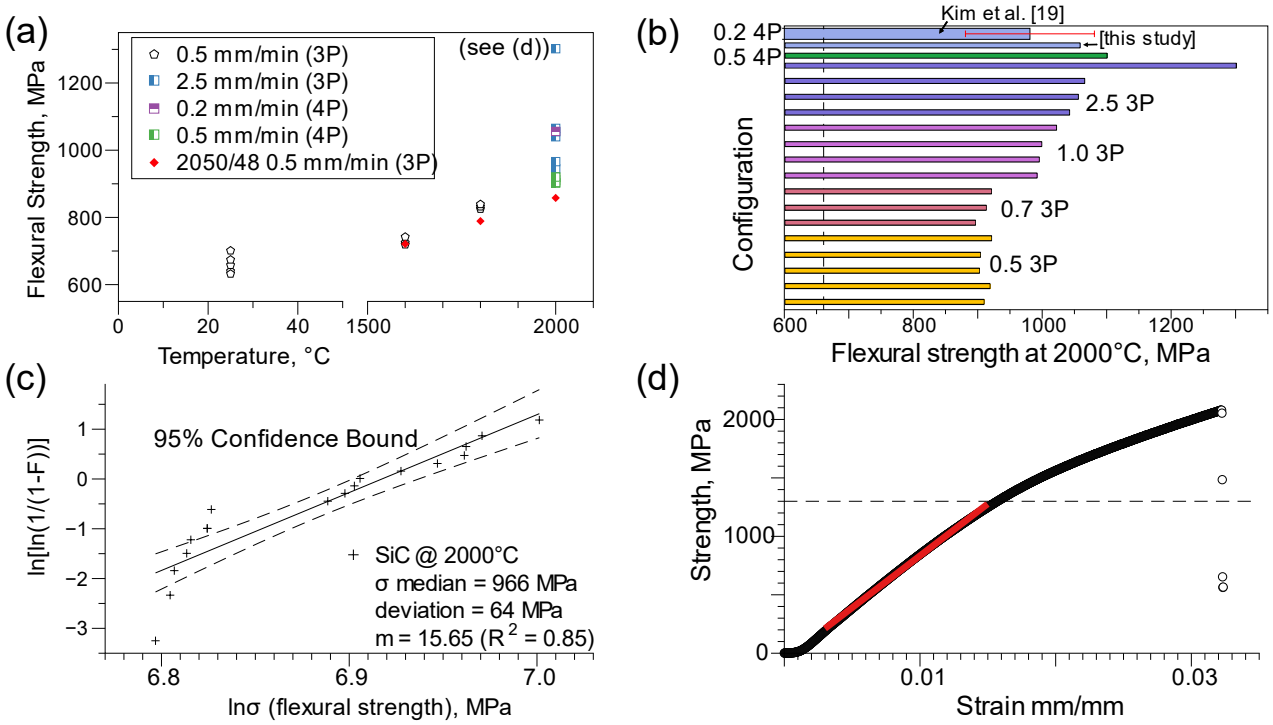

Figure 6: Flexural strength of silicon carbide bulks (2010/20) obtained in this study. (b) represents the strength data obtained at 2000°C using different configurations* in this study and by Kim et al. [19]. The dashed line in (b) is for the average strength at room temperature. (c) shows the Weibull plot for the 2000°C tests. (d) Loading curve for the α-SiC ceramic during the three-point flexural test using a 2.5 mm/min loading rate. The red line approximates a linear portion of the strain-stress curve. This specimen was later used for the TEM studies.

* 3P – three-point, 4P – four-point, numbers are loading rate in mm/min.

The data of Kim et al. [19] for the liquid phase sintered beta silicon carbide would have an unchanged strength up to 1800°C followed by an increase in strength at

2000°C. Within this study, we used the same equipment for flexural testing as Kim et al. [19] and, using α-SiC SPSed without any additives, found that strength would only slightly increase when compared to RT values vs 1600°C. However, we observed a gradual increase in strength above 1600°C. This increase in strength can be attributed to an increased contribution of plastic deformation during the tests. In [19] and within this study, the profound plastic curves were observed only at 2000°C. We also found that the strength and strain-stress curve of silicon carbide ceramics showed significant sensitivity to the strain rate (*see Section 3.4.2*). This agrees with Shinoda et al. [56], who reported even a superplastic deformation of SiC using the strain rate of 3×10^{-5} s^{-1}.

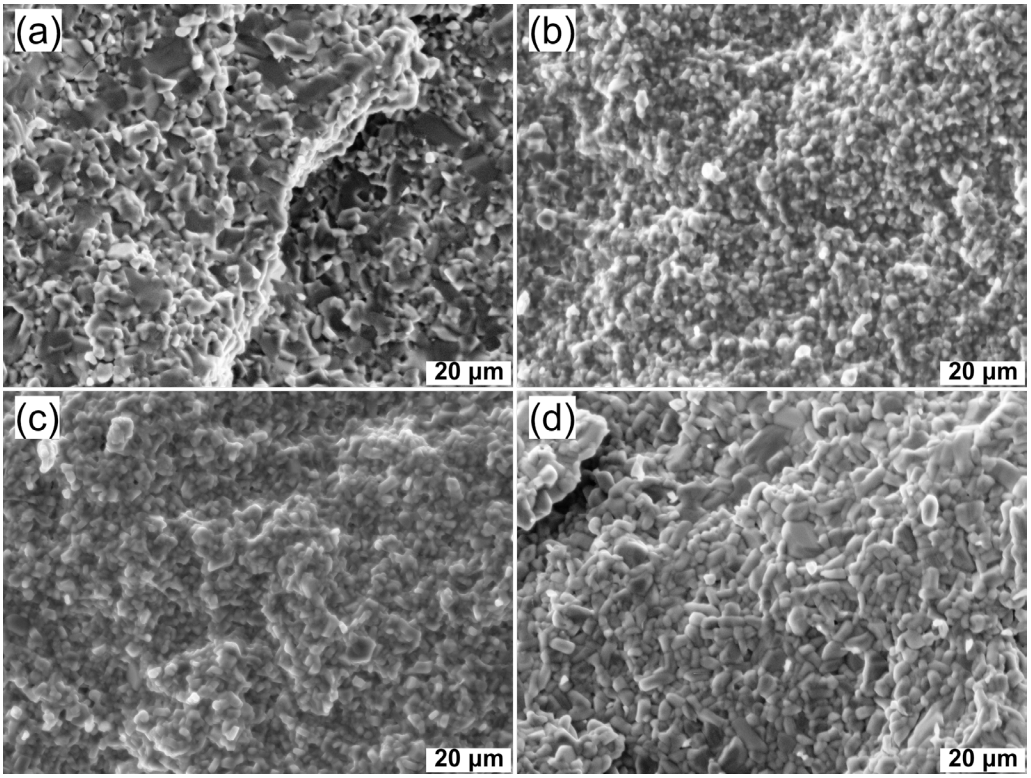

Figure 7: SEM images obtained from the fracture surface of the silicon carbide ceramics after bending tests at (a) 1600 °C, (b) 1800 °C, and (c, d) 2000 °C. (b, c) is for ceramic consolidated using a 2010/20 configuration, while (a, d) is for the specimen SPSed using 2050/48.

The effects of the loading conditions on the final strength are summarized in **Figure 6**. One can see that the strength exceeding 2 GPa was observed using the relatively high strain rate of 2.5 mm/min (also see *Suppl. S5*). The shape of the strain-stress curve had a peculiar shape (**Fig. 6(d)**), and the flexural strength reported in Fig. 8 is for the end of the elastic part of the strain-stress curve. One may recall that the theoretical strength of the silicon carbide E/10 would be around 40 GPa [57]; what is interesting here is that the elastic part would be as high as 1.3 GPa. Typical fracture surfaces after flexural tests suggested the dominance of the intergranular fracture as a main mechanism, as shown using secondary electron SEM images in **Fig. 7**.

The analysis of the densification mechanism (see section 3.2) suggested that the dislocation-based mechanism might be responsible for consolidation using spark plasma sintering. Thus, a sufficient number of dislocations and other defects, such as stacking faults, can be expected in as-consolidated ceramic. In this case, the high strength of bulk silicon carbide is due to 1) high bulk density, 2) absence of impurities, and 3) a fairly large number of defects. The relaxation of these defects and generation of novel defects during heating/flexure procedures is expected, as also reported in [55]. Hence, the TEM observations were carried out to identify the micro mechanism responsible for the increase of the flexural strength, particularly at 2000°C (*see section 3.4.3*).

3.4.2 Correlation between strain rate and the high-temperature deformation

First, to understand the mechanism behind the sensitivity of the flexural strength to the applied strain rate, we performed a formal analysis using a deformation map mechanism approach [58]. Using data from [1,5, 58] and Sargent and Ashby [59], we constructed the deformation maps for silicon carbide in **Fig. 8** (also see *Suppl. S*3). One can see that using a strain rate of 0.005 s^{-1} (0.5 mm/min) or 0.02 s^{-1} (2.5 mm/min), one should expect an increase in the stress. A similar observation was

experimentally confirmed for other ceramics [60]. According to [58], the ceramics fracture at a rate lower than 1×10^{-8} s^{-1} should be elastic, which is consistent with the result of this study, as plastic load-displacement curves were observed only at 2000°C.

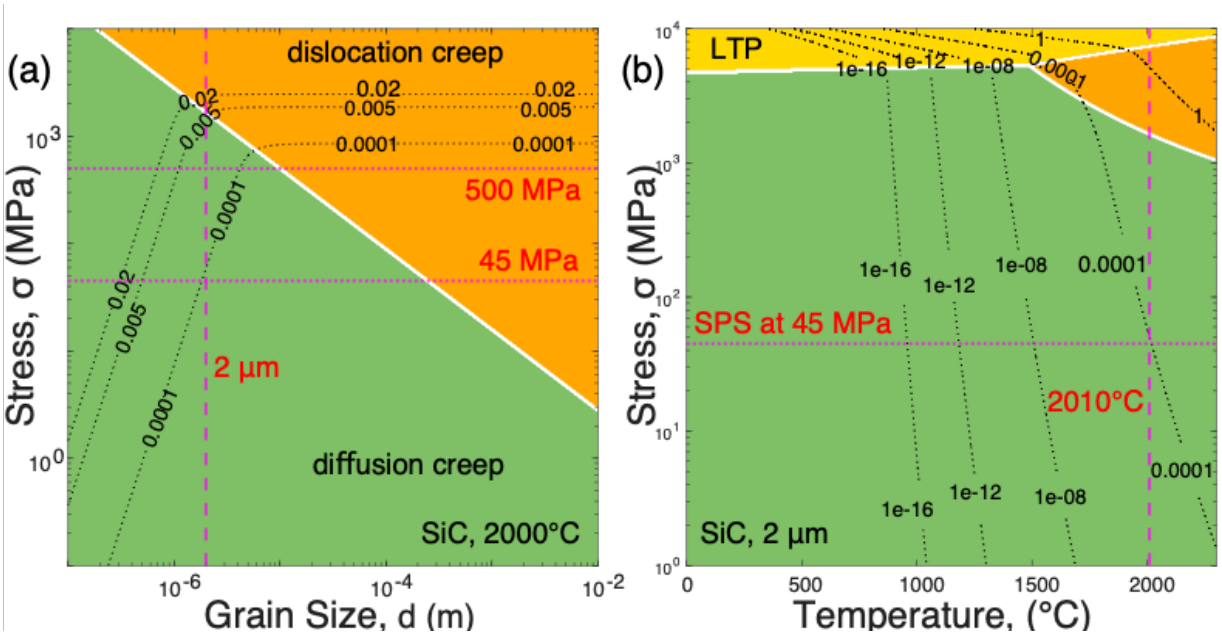

Figure 8: Deformation mechanism map for SiC: (a) at 2000 °C and (b) for the 2 µm grain size. Solid lines are for the combined strain rate in s^{-1}. Dashed lines are for the combined strain rate in s^{-1}. LTP – low-temperature plasticity.

It is worth noting that, similar to the strength, the fracture mechanism map can be expected [61]. Applying a slow loading rate above a certain temperature, i.e., 1600°C, will result in a relatively small area for the slow-crack growth region. For silicon nitride, Koehler et al. [62] suggested that the stress/strain rate increase may indirectly affect the strength. In contrast, the fracture toughness or crack propagation speed will be directly affected by the different strain rates. When a fixed temperature is maintained, an increase in strain rate should result in a corresponding increase in strength, assuming that the same mechanism is active, as depicted in **Figure 8**.

Here, we should stress that the ASTM C1211−13 indicates that the total time for the stress test should be between 10 and 40 seconds. In our tests, any temperature below 2000 °C this criterium is being satisfied using a 0.5 mm/min loading rate. At 2000°C,

a typical displacement-force curve using this rate will require up to 55 seconds to complete, and at the same time, at this loading rate, one always observes the plastic end after the linear elastic region. The same observation was made by Kim et al. [19]. Changing a set-up to four-point strength or using a configuration from B to A (i.e., 3×4×25 mm) will not change the shape of the curve. As one may expect, even a slight increase in loading rate, i.e., 0.7 or 1 mm/min, will ensure that the data collected are acceptable according to ASTM C1211−13. Hence, in this study, various loading rates were used to analyze strength at 2000°C (**Fig. 6**).

Crucially, an increase in the loading rate up to 5 mm/min (0.05 s^{-1}) would result in a completely linear loading curve, and it was not used in the analysis in **Fig. 6**, while the strength of nearly 1 GPa was observed. The fracture of these specimens remained identical to that of **Fig. 8(b)**. Hence, one may assume that a comparable crack growth speed was observed.

3.4.3 Local defects during the high-temperature deformation

We observed the microstructure of the 2010/20 sample after a flexural test at 2000°C from the undeformed (as-sintered) and highly deformed area (i.e., the tensile part in the vicinity of the crack formation) after a flexural test at 2000°C at the tensile side as the results are shown in **Figure 9**.

Fig. 9 (a) and (b) show the low and high magnification BF-TEM images obtained from undeformed area. One can observe the following: a) no visible cracks, b) the existence of twins in the grains. BF-STEM observations from the highly deformed area after the flexural test show the density of twins is substantially increased in the grains (**Fig. 9(c)**) while occasionally, the dislocations were present close to the grain boundary region (**Fig. 9(d)**). The SF always terminates within a grain, suggesting that this is an intrinsic strengthening mechanism and explains to some extent the ability to withstand stress exceeding 2 GPa (**Fig. 6 (d)**).

We did not observe any formation of an amorphous GB phase nor the segregation

of the secondary elements, as demonstrated in the high-resolution BF-STEM image shown in **Fig. 9(e, f)**. Maeda et al. [63] noted that relatively low SF energy for silicon carbide leads to extremely large dislocation width, provided that applied stress exceeds a critical level (~14 MPa).

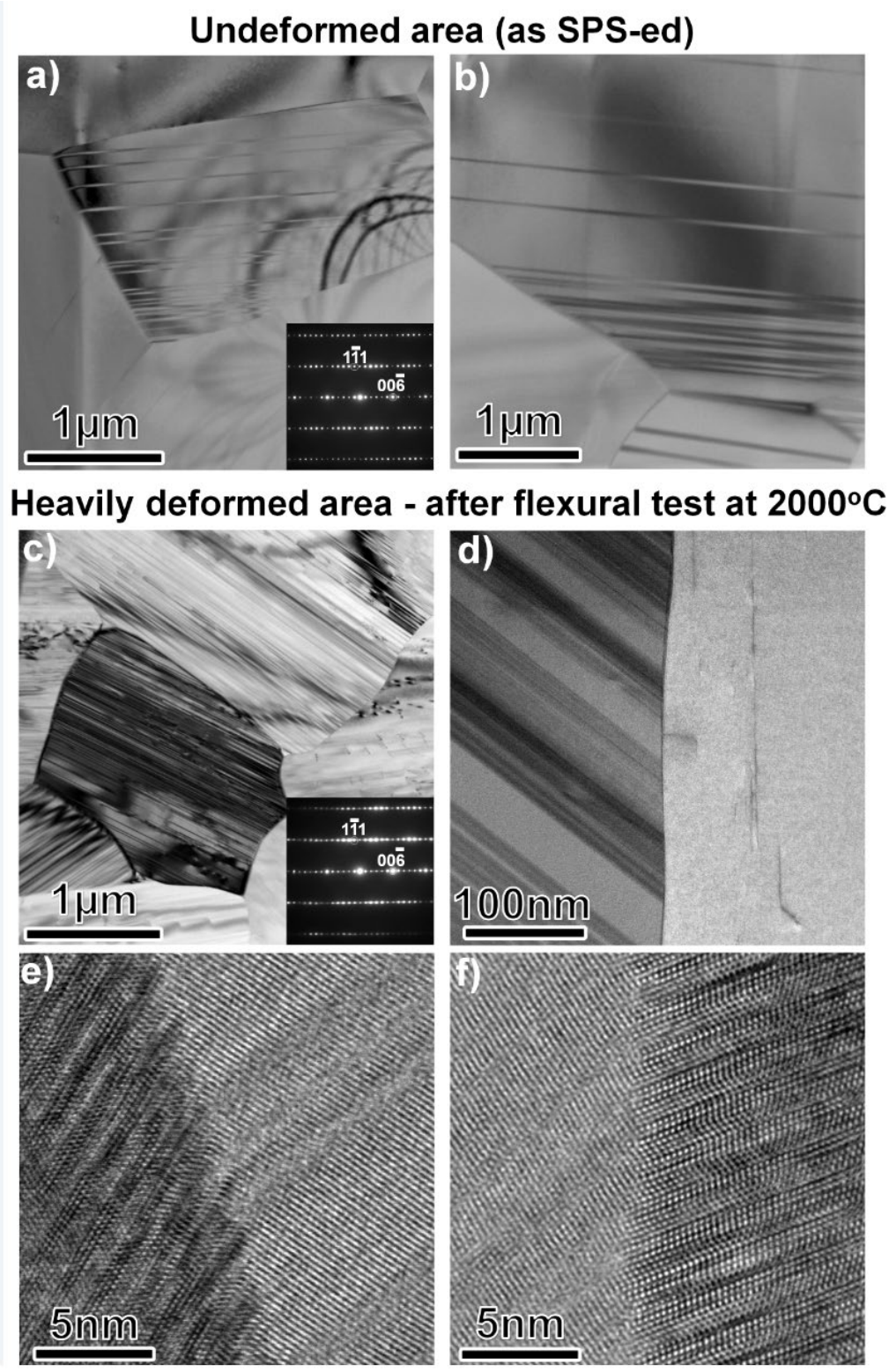

Figure 9: TEM observation of silicon carbide ceramics prepared within this study. (a-b) bright field (BF)-TEM image obtained from the 2010/20 sample prepared from undeformed (just SPSed) area and (c-f) overall microstructure of heavily deformed area after flexural test at 2000°C using a 2.5 mm/min loading rate. (c, d) BF-STEM images show the dislocation loops emitted from the center of the grains while the twinning plains are terminated at the grain boundaries. (e, f) A high-resolution BF-STEM image was obtained from a grain boundary region, illustrating the absence of an intergranular film. STEM-EDS data (not shown here) indicated no oxygen segregation in the grain boundaries of the as-SPSed or deformed materials.

This observation suggests that an accumulation of defects has occurred during the deformation process. As shown in **Fig. 9**, the twin density increase is most likely caused by the deformation during the flexural test. Here, one can consider that, in this case, the silicon carbide bulks illustrate a *self-strengthening* behavior at the nanoscale.

If numerous intergranular dislocations are observed in the deformed surface samples, these intergranular dislocations likely reveal that a grain boundary sliding mechanism operated during the deformation. However, we did not encounter a large amount of dislocation as expected for typical high-temperature plastic fracture, and, as a rule, stacking faults or twins were observed. These defects terminated inside the grains (**Fig. 9**). Suggesting that these defects (or the increase in density of these defects) are due to a release of internal stress during the deformation. Other processes, such as deformation-twinning, can also be considered [57]. However, this hypothesis cannot be confirmed for the specimen presented in **Fig. 9**.

The occurrence of plastic deformation was confirmed by the noticeable curvature in specimens tested at 1400°C. The temperature at which yielding was first observed coincided with the temperature at which the fracture stress began to increase. Thus,

it is reasonable to postulate that the same mechanism that led to yielding in bending also acted to relieve the stresses at the crack tip. As such, any increase in strength, as observed in **Fig. 9**, can be reasonably connected to the conclusions made by Gulden. Another similarity between the two studies is that CVD SiC [64] or additive-free polycrystalline SiC, as in this study, are reasonably pure, and oxide or any other phases will not affect the crack propagation process during the high-temperature deformation.

At this point, the structural performance of such produced SiC bulks can be further improved while focusing on toughness. As such, further studies that involve high-temperature toughness tests and optimization of the SPS processing to improve toughness are considered the next steps in the ongoing research, focusing mainly on the activation of the *self-strengthening* behavior at high temperatures.

Summary and concluding remarks

This study shows that a long-term dream of producing bulk additive-free silicon carbide was accomplished using a simple ramp-and-hold procedure at 2010°C using spark plasma sintering. bulk silicon carbide showed rather high hardness (29 GPa), room-temperature strength (600–700 MPa), and an acceptable level of toughness (2–3 MPa $m^{1/2}$).

Conditions for the consolidation of monolithic α-SiC ceramics were determined by optimization using an experimental design approach and statistical analysis of data on density, grain size, or 6H polytype content in the SPSed SiC bulk.

The consolidation of silicon carbide was analyzed similarly to the creep of bulk ceramics using the approach proposed by Bernard-Granger and Guizard [33]. It was established that the activation energy for the densification process is within 596±39 kJ/mol, which is in general agreement with previously reported studies on creep [48] or hot-pressing [10]. According to the stress exponent *n* value of 1.56 to 1.91, the mechanism responsible for the densification of silicon carbide without introducing

any additives into the system was the grain-boundary sliding or its combination with diffusional creep.

Nevertheless, dislocations were rarely observed for the ceramic after the SPS consolidation, and the main defects were stacking faults or twins. These defects were often terminated at the grain boundaries. Numerous probing attempts revealed that the grain boundaries for additive-free SiC were crystalline and contained no secondary or amorphous phases.

Importantly, SiC bulks showed a gradual increase in flexural strength from room temperature (>600 MPa) to 2000°C (>950 MPa). At least 10 measurements confirmed both values with a relatively high Weibull parameter ($m > 15$) for 2000 °C. At 2000°C, the flexural strength of additive-free SiC was sensitive to the loading rate, and under 2.5 mm/min, it reached a maximum of 2.08 GPa. To explain this observation, we used a constructed deformation mechanisms map [58], and it was found that the Coble creep is the most likely mechanism explaining the strain sensitivity of SiC at 2000°C. Furthermore, a gradual increase in strength with an increase in temperature for additive-free silicon carbide may be associated with the self-strengthening of this ceramic during the deformation process. We observed a sufficient increase in the stacking faults density inside the SiC grains at 2000°C, suggesting a self-strengthening mechanism was activated. Importantly, most twins and stacking faults terminate inside the grains, which can be connected to stress release during the deformation process.

Acknowledgments

The KAKENHI C 24K08035 Grant in Aids of Scientific Research partially supported this study. At TU, DD was supported by the World Premier International Research Center Initiative (WPI), MEXT (Japan), and Core Research Cluster for Materials Science, Tohoku University (Japan).

References

[1] T.Ya. Kosolapova, T.V. Andreeva, T.S. Bartnitskaya, et al., Non-metallic refractory compounds. Metallurgiya, Moscow, 1985. [in Russian].

[2] I.W. Edington, D.I. Rowcliffe, and I.L. Hensgall, The mechanical properties of silicon nitride and silicon carbide, Powder Met. Int., 7[3] (1975) 136–147.

[3] D. Demirskyi, O. Vasylkiv, Mechanical properties of SiC–NbB2 eutectic composites by in situ spark plasma sintering, Ceram. Int. 42 [16] (2016) 19372–19385. doi: https://doi.org/10.1016/j.ceramint.2016.09.110.

[4] M. Taya, S. Hayashi, A.S. Kobayashi, H.S. Yoon, Toughening of a particulate reinforced ceramic-matrix composite by thermal residual stress, J. Am. Ceram. Soc. 73 (1990) 1382–1391. doi: https://doi.org/10.1111/j.1151-2916.1990.tb05209.x.

[5] R.A. Andrievski, I.I. Spivak, Strength of Refractory Compounds. Metallurgiya, Chelyabinsk, 1989. [in Russian].

[6] R. Stevens, Defects in silicon carbide. J. Mater. Sci. 7 (1972) 517–521. doi: https://doi.org/10.1007/BF00761949.

[7] C. Greskovich, J.H. Rosolowski, Sintering of Covalent Solids, J. Am. Ceram. Soc. 59[7-8] (1976) 336–343. doi: https://doi.org/10.1111/j.1151-2916.1976.tb10979.x.

[8] J.B. Hurst, S. Dutta, Simple Processing Method for High-Strength Silicon Carbide, J. Am. Ceram. Soc. 70[11] (1987) C-303–C-308. doi: https://doi.org/10.1111/j.1151-2916.1987.tb05642.x.

[9] S. Dutta, Densification and Properties of α-Silicon Carbide, J. Am. Ceram. Soc. 68[10] (1985) C-269–C-270. doi: https://doi.org/10.1111/j.1151-2916.1985.tb11527.x.

[10] M. Lodhe, N. Chawake, D. Yadav, M. Balasubramanian, On correlation between β → α transformation and densification mechanisms in SiC during spark plasma sintering, Scr. Mater. 115 (2016) 137 – 140. doi: https://doi.org/10.1016/j.scriptamat.2016.01.002.

[11] R. Vaßen, A. Kaiser, J. Förster, H.P. Buchkremer, D. Stöver, Densification of ultrafine SiC powders, J. Mater. Sci. 31 (1996) 3623–3637. doi: https://doi.org/10.1007/BF00352770.

[12] H. Tanaka, Y. Zhou, Low temperature sintering and elongated grain growth of 6H-SiC powder with AlB2 and C additives, J. Mater. Res. 14 [2] (1999) 518–522. doi: https://doi.org/10.1557/JMR.1999.0074.

[13] Y.-W. Kim, S. Kultayeva, J. Sedlacek, O. Hanzel, P. Tatarko, et al., Thermal and electrical properties of additive-free rapidly hot-pressed SiC ceramics, J. Eur. Ceram. Soc. 40[2] (2020) 234–240. doi: https://doi.org/10.1016/j.jeurceramsoc.2019.10.015.

[14] R.A. Alliegro, L.B. Coffin, J.R. Tinklepaugh, Pressure-Sintered Silicon Carbide, J. Am. Ceram. Soc. 39[11] (1956) 386–389. doi: https://doi.org/10.1111/j.1151-2916.1956.tb15609.x.

[15] J.M. Bind, J.V. Biggers, Hot-Pressing of Silicon Carbide with 1% Boron Carbide Addition, J. Am. Ceram. Soc. 58[7-8] (1975) 304–306. doi: https://doi.org/10.1111/j.1151-2916.1975.tb11482.x.

[16] D. Demirskyi, O. Vasylkiv, Hot-spots generation, exaggerated grain growth and mechanical performance of silicon carbide bulks consolidated by flash spark plasma sintering, J. Alloys Compd. 691 (2017) 466–473. doi: https://doi.org/10.1016/j.jallcom.2016.08.234.

[17] S. Prochazka, R.M. Scanlan, Effect of Boron and Carbon on Sintering of SiC, J. Am. Ceram. Soc. 58[1-2] (1975) 72. doi: https://doi.org/10.1111/j.1151-2916.1975.tb18990.x.

[18] T. Yamamoto, H. Kitaura, Y. Kodera, T. Ishii, M. Ohyanagi, Z.A. Munir, Consolidation of Nanostructured β-SiC by Spark Plasma Sintering, J. Am. Ceram. Soc. 87[8] (2004) 1436–1441. doi: https://doi.org/10.1111/j.1551-2916.2004.01436.x.

[19] Y.W. Kim, S.-H. Jang, T. Nishimura, S.-Y. Choi, S.-D. Kim, Microstructure and high-temperature strength of silicon carbide with 2000 ppm yttria, J. Eur. Ceram.

Soc. 37[15] (2017) 4449–4455. doi: https://doi.org/10.1016/j.jeurceramsoc.2017.07.002.

[20] P. Sajgalik, J. Sedlacek, Z. Lencez, J. Dusza, H.-T. Lin, Additive-free hot-pressed silicon carbide ceramics - A material with exceptional mechanical properties, J. Eur. Ceram. Soc. 36[6] (2016) 1333–1341. doi: https://doi.org/10.1016/j.jeurceramsoc.2017.07.002.

[21] A. Maitre, A. Vande Put, J.P. Laval, S. Valette, G. Trolliard, Role of boron on the Spark Plasma Sintering of an α-SiC powder, J. Eur. Ceram. Soc. 28[9] (2008) 1881–1890. doi: https://doi.org/10.1016/j.jeurceramsoc.2008.01.002.

[22] F.C. Leone, N.L. Johnson, Statistics and Experimental Design In Engineering and the Physical Sciences, Vol 2, John Wiley and Sons, N.Y., 1964.

[23] M.H. Quenouille, The Design and Analysis of Experiment, New York, Hafner Publishing Company, 1953.

[24] N.P. Klepieov, S.N. Sokolov, Analysis and Design of Experiments by the Maximum Likelihood Method, Nauka, Moscow, 1964. [in Russian].

[25] D. Demirskyi, O. Vasylkiv, Consolidation and grain growth of tantalum diboride during spark plasma sintering, Ceram. Int. 42[14] (2016) 16396–16400. https://doi.org/10.1016/j.ceramint.2016.07.059.

[26] D. Demirskyi, T.S. Suzuki, K. Yoshimi, O. Vasylkiv, Consolidation and high-temperature strength of monolithic lanthanum hexaboride, J. Am. Ceram. Soc. 105[6] (2022) 4277–4290. doi: https://doi.org/10.1111/jace.18331.

[27] N. Doebelin, R. Kleeberg, Profex: a graphical user interface for the Rietveld refinement program BGMN, J. Appl. Cryst. 48 (2015) 1573–1580. doi: https://doi.org/10.1107/S1600576715014685.

[28] D. Demirskyi, O. Vasylkiv, Analysis of the high-temperature flexural strength behavior of B4C–TaB2 eutectic composites produced by in situ spark plasma sintering, Mater. Sci. Eng. A 697 (2017) 71–78. doi: https://doi.org/ 10.1016/j.msea.2017.04.093.

[xx] D. Demirskyi, O. Vasylkiv, K. Yoshimi, Allotropic strengthening and in situ

phase transformations during ultra-high-temperature flexure of bulk tantalum nitride, Mater. Sci. Eng. A 826 (2021) 141954. doi: https://doi.org/10.1016/j.msea.2021.141954.

[29] G.R. Anstis, P. Chantikul, B.R. Lawn, D.B. Marshall, A critical evaluation of 1ndentation techniques for measuring fracture toughness: I, direct crack measurements, J. Am. Ceram. Soc. 64[9] (1981) 533–538. doi: https://doi.org/10.1111/j.1151-2916.1981.tb10320.x.

[30] B.R. Lawn, E.R. Fuller, Equilibrium penny-like cracks in indentation fracture. J. Mater. Sci. 10 (1975) 2016–2024. https://doi.org/10.1007/BF00557479.

[31] S. Grasso, T. Saunders, H. Porwal, B. Milsom, A. Tudball, M. Reece, Flash Spark Plasma Sintering (FSPS) of α and β SiC, J. Am. Ceram. Soc. 99[5] (2016) 1534–1543. doi: https://doi.org/10.1111/jace.14158.

[32] P. Murray. E. P.Roders, A.E. Williams, Practical and Theoretica1 Aspects of the Hot Pressing of Refractory Oxides, Trans. Brit. Ceram. Soc., 53[8] (1954) 474–510.

[33] G. Bernard-Granger, C. Guizard, Spark plasma sintering of a commercially available granulated zirconia powder: I. Sintering path and hypotheses about the mechanism(s) controlling densification, Acta Mater. 44[10] (2007):3493–3504. doi: https://doi.org/10.1016/j.actamat.2007.01.048.

[34] S. Sameshima, K. Miyano, Y. Hirata, Sinterability of SiC powder coated uniformly with Al ions, J. Mater. Res. 13 (1998) 816–820. doi: https://doi.org/10.1557/JMR.1998.0104.

[35] B. Burton, The characteristic equation for superplastic flow, Phil. Mag. A 48 (1983) L9–L13. doi: https://doi.org/10.1080/01418618308234906.

[36] T.G. Langdon, Grain boundary sliding revisited: Developments in sliding over four decades, J. Mater. Sci. 41 (2006) 597–609. doi: https://doi.org/10.1007/s10853-006-6476-0.

[37] W.R. Cannon, O.D. Sherby, Creep Behavior and Grain-Boundary Sliding in Polycrystalline Al2O3, J. Am. Ceram. Soc. 60[1-2] (1977) 44–47. doi:

https://doi.org/10.1111/j.1151-2916.1977.tb16090.x.
[38] M.F. Ashby, R.A. Verrall, Diffusion-Accommodated Flow and Superplasticity, Acta Metall. 21[2] (1973) 149–163. doi: https://doi.org/10.1016/0001-6160(73)90057-6.
[39] V.A. Philips, J.A. Hugo, The resolution of lattice planes and lattice defects in semiconductors including observations on boundaries, Acta Metall. 18 (1970) 123–135. doi: https://doi.org/10.1016/0001-6160(70)90076-3.
[40] D. Demirskyi, H. Sepehri-Amin, T.S.Suzuk, K.Yoshimi, O.Vasylkiv, Ultra-high temperature flexure and strain driven amorphization in polycrystalline boron carbide, Scr. Meter. 210 (2022) 114487. doi: https://doi.org/10.1016/j.scriptamat.2021.114487.
[41] S. Zhao, R. Flanagan, E.N. Hahn, B. Kad, B.A. Remington, C.E. Wehrenberg, et al., Shock-induced amorphization in silicon carbide, Acta Mater. 158 (2018) 206–213, doi: https://doi.org/10.1016/j.actamat.2018.07.047.
[42] W. van Rijswijk, D.J. Shanefield, Effects of carbon as a sintering aid in silicon carbide, J. Am. Ceram. Soc. 73[1] (1990) 148–149. doi: https://doi.org/10.1111/j.1151-2916.1990.tb05109.x.
[43] J.E. Lane, C.H. Carter Jr., R.F. Davis, Kinetics and Mechanisms of High-Temperature Creep in Silicon Carbide: III, Sintered a-Silicon Carbide, J. Am. Ceram. Soc. 71[4] (1988) 281–295. doi: https://doi.org/10.1111/j.1151-2916.1988.tb05861.x.
[44] R.D. Nixon, R.F. Davis, Diffusion-Accommodated Crain Boundary SIiding and Dislocation Glide in the Creep of Sintered Alpha Silicon Carbide, J. Am. Ceram. Soc. 75[7] (1992) 1786–1795. doi: https://doi.org/10.1111/j.1151-2916.1992.tb07198.x.
[45] C.H. Carter, R.F. Davis, Kinetics and Mechanisms of High-Temperature Creep in Silicon Carbide: II, Chemically Vapor Deposited, J. Am. Ceram. Soc. 67[11] (1984) 732–740. doi: https://doi.org/10.1111/j.1151-2916.1984.tb19510.x.
[46] H. Tanaka, Y. Inomata, Diffusional Creep in Sintered Silicon Carbide, J. Jpn.

Ceram. Soc, 93[1] (1985) 45–50 doi: https://doi.org/10.2109/jcersj1950.93.55.

[47] V. Krishnamachari, M.R. Notis, Interpretation of High-temperature Creep of SiC by Deformation Mapping Techniques, Mater. Sci. Eng. 27[1] (1977) 83–88. doi: https://doi.org/10.1016/0025-5416(77)90198-7.

[48] P.L. Farnsworth, R.L. Coble, Deformation Behavior of Dense Polycrystalline SiC. J. Am. Ceram. Soc. 49[5] (1966) 264–268. doi: https://doi.org/10.1111/j.1151-2916.1966.tb13254.x.

[49] T.L. Francis, R.L. Coble, Creep of Polycrystalline Silicon Carbide, J. Am. Ceram. Soc. 51[2] (1968) 115–116. doi: https://doi.org/10.1111/j.1151-2916.1968.tb11853.x.

[50] S.G. Seshadrani, D.M. Srinivasa, Estimation of Fracture Toughness by Intrinsic Flaw Fractography for Sintered Alpha Silicon Carbide, J. Am. Ceram. Soc. 64[4] (1981) c69–c71. doi: https://doi.org/10.1111/j.1151-2916.1981.tb10284.x.

[51] H. Tanaka, Sintering of silicon carbide, in: S. Somiya, Y. Inomata (Eds.), Silicon Carbide Ceramics, Elsevier Applied Science, London, 1991, pp. 213–238. doi: https://doi.org/10.1007/978-94-011-3842-0_10.

[52] C.H. McMurtry, W.D.G. Boecker, S.G. Seshadri, J.S. Zanghi, J.E. Garnier, Microstructure and material properties SiC−TiB2 particulate composites, Bull. Am. Ceram. Soc. 66 (1987) 325–329.

[53] Sixta, M.E. Creep of SiC Hot-Pressed with Al, B, and C. Ph.D. thesis, University of California, Berkeley, CA, US, 2000. doi: https://doi.org/10.2172/764381.

[54] H.C. Chandan, L. Hermansson, H. Abe, R.C. Bradt, Elevated temperature instrumented Charpy impact of a sintered silicon carbide, Ceram. Int. 9[4] (1983) 114–118. doi: https://doi.org/10.1016/0272-8842(83)90010-X.

[55] O. Vasylkiv, D. Demirskyi, H. Borodianska, A. Kuncser, P.Badica, High-temperature strength of boron carbide with Pt grain-boundary framework in situ synthesized during spark plasma sintering, Ceram. Int. 46 [7] (2020) 9136–9144. doi: https://doi.org/10.1016/j.ceramint.2019.12.163.

[56] Y. Shinoda, T. Nagano, H. Gu, F. Wakai, Superplasticity of Silicon Carbide, J. Am. Ceram. Soc. 82[10] (1999) 2916–2918. doi: https://doi.org/10.1111/j.1151-2916.1999.tb02178.x.

[57] Th.H. Courtney. Mechanical Behavior of Materials, 2nd Edition, Waveland Press, 2005.

[58] H.J. Frost, M.F. Ashby, Deformation-Mechanism Maps: The Plasticity and Creep of Metals and Ceramics, Pargamon Press, Oxford, 1982.

[59] P.M. Sargent, M.F. Ashby, Deformation-Mechanism Maps for SiC, Scr. Metall. 17[7] (1983) 951–957.

[60] S.R. Choi, J.P. Gyekenyesi, "Ultra"-Fast Fracture Strength of Advanced Structural Ceramics at Elevated Temperatures: An Approach to High-Temperature 'Inert' Strength. In: R.C. Bradt, D. Munz, M. Sakai, V.Y. Shevchenko, K. White, K. (eds.) Fracture Mechanics of Ceramics. Springer, Boston, MA, 2002, pp. 27–46. doi: https://doi.org/10.1007/978-1-4757-4019-6_3.

[61] G.D. Quinn, W.R. Braue, Fracture mechanism maps for advanced structural ceramics. Part 2 Sintered silicon nitride, J. Mater. Sci. 25 (1990) 4377–4392. doi: https://doi.org/10.1007/BF00581097.

[62] N. Kohler, Y. Ikuhara, H. Awaji, K. Funatani, High Temperature Fracture Mechanism of Gas-Pressure Sintered Silicon Nitride. In: R.C. Bradt, D.P.H. Hasselman, D. Munz, M. Sakai, V.Y. Shevchenko, V.Y. (eds.) Fracture Mechanics of Ceramics. Fracture Mechanics of Ceramics, vol 10. Springer, Boston, MA, 1992, pp. 367–377. doi: https://doi.org/10.1007/978-1-4615-3348-1_24.

[63] K. Maeda, K. Suzuki, S. Fujita, M. Ichihara, S. Hyodo, Defects in plastically deformed 6H SiC single crystals studied by transmission electron microscopy, Phil. Mag. A 57[4] (1988) 573–592. doi: https://doi.org/10.1080/01418618808214408.

[64] T.D. Gulden, Mechanical Properties of Polycrystalline β-SiC, J. Am. Ceram. Soc. 52[11] (1969) 585–590. doi: https://doi.org/10.1111/j.1151-2916.1969.tb15845.x.